







# Cryogenic 3D Printing of GelMA/Graphene Bioinks: Improved Mechanical Strength and Structural Properties for Tissue Engineering

Moises das Virgens Santana <sup>1</sup>, Maria Beatriz S Magulas <sup>1</sup>, Guilherme Castro Brito<sup>1</sup>, Mariana Chaves Santos<sup>1</sup>, Tainara Gomes de Oliveira<sup>1</sup>, Wanderson Gabriel Gomes de Melo <sup>2</sup>, Napoleao Martins Argolo Neto<sup>2</sup>, Fernanda Roberta Marciano <sup>1,3</sup>, Bartolomeu Cruz Viana <sup>1,3</sup>, Anderson Oliveira Lobo <sup>1</sup>

<sup>1</sup>LIMAV-Interdisciplinary Laboratory for Advanced Materials, UFPI - Federal University of Piauí, Teresina, PI, 64049-550, Brazil; <sup>2</sup>Integrated Center for Morphology and Stem Cell Research, Postgraduate Program in Technologies Applied to Animals of Regional Interest, Federal University of Piauí, Teresina, PI, 64049-550, Brazil; <sup>3</sup>Department of Physics, UFPI - Federal University of Piauí, Teresina, PI, 64049-550, Brazil

Correspondence: Anderson Oliveira Lobo, Email [lobo@ufpi.edu.br](mailto:lobo@ufpi.edu.br)

**Purpose:** Tissue engineering aims to recreate natural cellular environments to facilitate tissue regeneration. Gelatin methacrylate (GelMA) is widely utilized for its biocompatibility, ability to support cell adhesion and proliferation, and adjustable mechanical characteristics. This study developed a GelMA and graphene bioink platform at concentrations of 1, 1.5, and 2 mg/mL to enhance scaffold properties for tissue engineering applications.

**Patients and Methods:** Graphene was incorporated into GelMA matrices to improve mechanical strength and electrical conductivity of the bioinks. The compressive strength and thermal stability of the resulting GelMA/graphene scaffolds were assessed through DSC analysis and mechanical testing. Cytotoxicity assays were conducted to determine cell survival rates. Cryoprinting at  $-30^{\circ}\text{C}$  was employed to preserve scaffold structure and function. The chorioallantoic membrane (CAM) assay was used to evaluate biocompatibility and angiogenic potential.

**Results:** The integration of graphene significantly amplified the compressive strength and thermal stability of GelMA scaffolds. Cytotoxicity assays indicated robust cell survival rates of 90%, confirming the biocompatibility of the developed materials. Cryoprinting effectively preserved scaffold integrity and functionality. The CAM assay validated the biocompatibility and angiogenic potential, demonstrating substantial vascularization upon scaffold implantation onto chick embryo CAM.

**Conclusion:** Integrating graphene into GelMA hydrogels, coupled with low-temperature 3D printing, represents a potent strategy for enhancing scaffold fabrication. The resultant GelMA/graphene scaffolds exhibit superior mechanical properties, biocompatibility, and pro-vascularization capabilities, making them highly suitable for diverse tissue engineering and regenerative medicine applications.

**Keywords:** GelMA, graphene, cryoprinting, hydrogels and tissue engineering

## Introduction

Tissue engineering aims to recreate the natural cellular environment to effectively promote tissue regeneration. GelMA (gelatin methacrylate) is widely used as a biomaterial due to its biocompatibility, its ability to support cell adhesion and proliferation, and its adjustable mechanical properties.<sup>1-3</sup> The addition of graphene to these hydrogel matrices opens new possibilities in bioengineering by enhancing the capabilities of bioinks through improved mechanical properties and electrical conductivity.<sup>4,5</sup> Graphene, with its unique properties such as strength, flexibility and electrical conductivity, improves the properties of GelMA and creates an even more favorable environment for cell growth and differentiation.<sup>4,6</sup>

Despite its promising properties, the use of graphene faces major challenges. Studies indicate that the biocompatibility of graphene can vary greatly depending on its functionalization and the presence of impurities. For example, non-functionalized graphene can trigger inflammatory reactions and cytotoxicity at concentrations above 20  $\mu\text{g/mL}$ .<sup>6,7</sup> These

problems limit the clinical applicability of graphene and require further studies to understand the mechanisms of toxicity and improve its safety.<sup>8</sup> The integration of graphene into GelMA results in hydrogels with improved mechanical properties, including increased elastic modulus and fracture resistance.<sup>9</sup> Studies show that the addition of graphene oxide (GO) can increase toughness without compromising the flexibility of the hydrogel and facilitates the restoration of hydrogen bonds after deformation.<sup>8,9</sup> The porosity of these composites is also adjustable, which is critical for nutrient diffusion and cell growth within the 3D matrices.<sup>2,6</sup>

In the current literature, the combination of GelMA with graphene oxide (GO) is being investigated due to its improved biocompatibility and mechanical properties. For example, GelMA/GO hydrogels have been used for progenitor cell differentiation and bone regeneration and have shown promising results in the development of bone tissue.<sup>7,8</sup> The specific combination of GelMA with pure graphene is less explored, possibly due to biocompatibility concerns and the difficult handling of pure graphene forms.<sup>10</sup> The interaction between GelMA and graphene is expected to promote a biocompatible matrix that supports not only cell adhesion and proliferation, but also differentiation and tissue regeneration due to the conductive properties of graphene. This combination may be particularly beneficial for applications that require structural support and electrical signaling, such as cardiac and neural tissue regeneration.<sup>9,11</sup>

The integration of GelMA into cryobioprinting has the potential to create highly organized and functional structures that are essential for engineering technologies.<sup>11</sup> Cryobioprinting is an emerging technique in biofabrication that utilizes low temperatures to print complex biological structures. This method enables the preservation of cellular predictions and structural integrity of biomaterials during and after the printing process.<sup>12</sup> Studies have shown that cryoprinting of GelMA results in structures with superior mechanical and biological properties and promotes cell proliferation.<sup>11,12</sup> Therefore, the low-temperature environment of cryoprinting minimizes thermal damage to cells and maintains conductive properties when using graphene, which are critical for cardiac and neural tissue engineering applications. In this work, we have developed a low temperature printed bioink platform based on GelMA/graphene at different concentrations (GelMA/GR) for tissue engineering applications with the aim of creating structures that support cell growth and promote effective tissue regeneration.

## Materials and Methods

### Materials

The materials used were porcine skin gelatin (Sigma-Aldrich, type A, 300 bloom,  $\geq 98\%$ , CAS: [9000–70–8]), photoinitiator 2-hydroxy-1-[4-(hydroxyethoxy) phenyl] –2-methyl-1-propanone (Irgacure 2959) (Sigma-Aldrich, CAS: [1,076,797–53–9],  $\geq 98\%$ ), phosphate-buffered saline (PBS) (Sigma-Aldrich,  $\geq 97\%$ ), methacrylic anhydride (MA) (Sigma-Aldrich,  $\geq 99\%$ , CAS: [760–93–0]), Xtra Performance (XP) graphene powder with a specific surface area of 100–140 m<sup>2</sup>/g and an average lateral size of 1–2  $\mu\text{m}$  (2DM Solutions, CAS: [1,034,343–98–0]), dialysis membrane (12–14 KDA) (SERVAPOR<sup>®</sup>), and distilled water.

### Gelma Synthesis

GelMA synthesis was performed according to the protocol described in a previous work.<sup>13</sup> In brief, 10 g of gelatin from pig skin was dissolved in 100 mL of PBS solution in a magnetic stirrer and heated at 50°C for 60 min. Methacrylic anhydride was then slowly added dropwise. The solution was stirred at 50°C for 3 hours. Subsequently, 200 mL of PBS was added to the mixture and the solution was filtered three times with a vacuum pump. Finally, dialysis was performed for 7 days using 12–14 KDA dialysis membranes, changing the solution every 24 hours with distilled water to remove unreacted anhydride. The solution was then frozen at –18°C and freeze-dried using an LS3000-Terroni freeze dryer (São Carlos/SP) LSX000 series, version 3.0/2014 for 5 days and then used.

### Bioink Design and Printing of Bioink

GR was added at different concentrations (1; 1.5; 2 mg/mL) to 10 mL of PBS solution and then sonicated at 80 W for 10 minutes in a probe sonicator. The GR dispersion in PBS was then added to GelMA (10% w/v) and heated in a water bath at 50°C for 30 minutes. Porcine skin gelatin (5% w/v) was then added, followed by incorporation of Irgacure (1% w/v). The

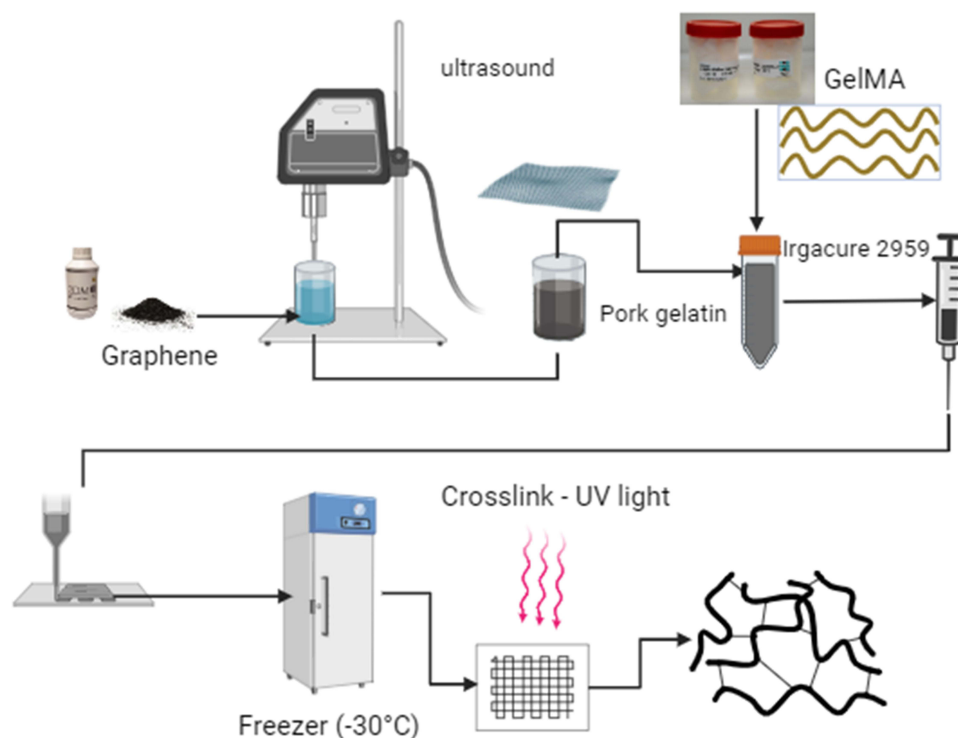


**Figure 1** Flowchart with the methodology developed for production and 3D printing of scaffolding.

solution was kept at 50°C for 30 minutes in a closed container wrapped in aluminum foil to protect it from light, with shaking every 10 minutes for 1 minute. This methodology is shown schematically in Figure 1.

The bioinks were printed using an Allevi 2 3D bioprinter with a pressure of 20–40 Psi and 25 Gauge needles. For low-temperature printing, the materials were printed on a Peltier plate at –30°C and then placed in a freezer at –30°C for 2 hours to ensure uniform temperature throughout the material. After that, the material was crosslinked for 5 minutes in a UV light chamber with a wavelength of 365 nm. The formulations with their respective abbreviations are described in Table 1.

**Table 1** Nomenclature Adopted for Each Studied Group

Nomenclature	Acronym
Methacrylated gelatin	GelMA
Low temperature printed methacrylated gelatin	GelMA-BT
Methacrylated gelatin and Graphene 1 mg/mL	GelMA-GR1
Methacrylated gelatin and Graphene 1.5 mg/mL	GelMA-GR1.5
Methacrylated gelatin and Graphene 2 mg/mL	GelMA-GR2
Methacrylated Gelatin and Graphene 1 mg/mL printed at low temperature	GelMA-BT-GR1
Methacrylated Gelatin and Graphene 1.5 mg/mL printed at low temperature	GelMA-BT-GR1.5
Methacrylated Gelatin and Graphene 2 mg/mL printed at low temperature	GelMA-BT-GR2
Methacrylated Gelatin and Graphene 2 mg/mL printed at low temperature and Cell	GelMA-BT-GR2 <sup>#</sup>

## Characterizations

### X-Ray Diffraction

The X-ray diffraction pattern of graphene and the scaffolds was obtained using a Shimadzu XRD-6000 diffractometer with CuK $\alpha$  radiation, a current of 30 mA, a scanning speed of 1°/min, and a ranged at 2 $\theta$  from 5° to 80°.

### Fourier Transform Infrared Spectroscopy

To analyze the chemical groups obtained through GR incorporation, the different formulations were subjected to Fourier Transform Infrared Spectroscopy, using the FTIR-ATR mode (VERTEX 70 BRUKER). The spectra were obtained in the range of 600 to 4500 cm<sup>-1</sup>.

### Differential Scanning Calorimetry

The thermal properties were analyzed using Differential Scanning Calorimetry (DSC). The characterization was performed using a Shimadzu DSC-60 analyzer. The scanning temperature used was 600°C at a heating rate of 20°C/min under a nitrogen atmosphere.

### Scanning Electron Microscopy

Micrographs were obtained using a FEI Quanta 250 scanning electron microscope (SEM) with a voltage of 10 KV, equipped with an Energy Dispersive X-ray (EDS) microanalysis system, Bruker Xflash 4030 with SDD (Silicon Drift Detector).

### Mechanical Tests

The compressive mechanical properties of the scaffolds were obtained using a NanoMec 50 – Hsensor mechanical testing equipment (50N load cell) at a constant speed of 1 mm/min. All samples were tested in triplicate.

### Toxicity Test

The in vitro cytotoxicity test of the scaffolds was performed using the Artemia salina nauplii lethality method. The samples were immersed in test tubes in artificial seawater with different concentrations of the material (0.1–5 mg/mL). After hatching, the number of live and dead nauplii was counted after 24 and 48 hours, also taking into account the negative and positive controls carried out with dimethyl sulfoxide (DMSO) and artificial seawater, respectively.

### Extrusion Evaluation for 3D Printing

To perform the injectability test (extrusion evaluation for 3D printing), GelMA formulations and GelMA with different graphene concentrations (1 mg/mL, 1.5 mg/mL, 2 mg/mL) were prepared according to the standard protocol. The system was then set up, which consisted of a 10 mL syringe with a 15 mm column of the material. The device used for the test was the NanoMec 50 – Hsensor, set to a displacement of 1 mm per minute, with a 50 N load cell. The behavior of the material was also visually observed during the test to assess the uniformity of the flow and detect any obstructions or inconsistencies. After the test, the recorded data was analyzed to determine the force required to extrude each GelMA formulation relative to the displacement from the syringe.

## Cytotoxicity Evaluation of GelMA and Graphene-Based Hydrogels in L929

### Cells and Animals' Facilities

The cells used were murine fibroblasts (L-929), previously isolated and cryopreserved. All procedures were approved by the Committee on Animal Research at Federal University of Piauí (UFPI) (N° 686/2021) and followed Brazilian (Colégio Brasileiro de Experimentação Animal - COBEA) and International rules on the care and use of experimental animals (Directive 2010/63/EU of the European Parliament and of the Council on the protection of animals used for scientific purposes).

Murine axillary lymph node endothelium-like cell lines (SVEC4-10) and murine fibroblasts (L-929) were cultured in DMEM and high glucose DMEM media, supplemented with 10% fetal bovine serum and 1% (w/v) penicillin/streptomycin. The cultures, containing  $2 \times 10^6$  viable cells, were incubated in flasks at 37°C, with 95% humidity and 5% CO<sub>2</sub> atmosphere (Shel Lab CO<sub>2</sub> Incubator, USA) at the Cancer Laboratory, UFPI, Teresina, Brazil.



Spontaneously hypertensive (SHR) female Wistar rats (*Rattus norvegicus*), weighing between 180 and 200 g, were obtained from the Central Animal Facility at the Federal University of Piauí (UFPI), Teresina, Brazil. They were housed in well-ventilated cages under standard light conditions (12-hour light/dark cycle) and temperature ( $22 \pm 1^\circ\text{C}$ ), with access to commercial rodent chow (Nutrilabor, Campinas, Brazil) and water ad libitum.

### Experimental Design

Nine hydrogels (GelMA, GelMA/GR1, GelMA-GR1.5, GelMA-GR2, GelMA-BT, GelMA-BT-GR1, GelMA-BT-GR1.5, GelMA-BT-GR2 and GelMA-BT-GR2<sup>#</sup>) were tested for their cytotoxic potential against murine fibroblasts L929. The L929 cells were cultured in complete Dulbecco's Modified Eagle Medium (DMEM) supplemented with 15% fetal bovine serum (FBS), 1% L-glutamine, 1% non-essential amino acids and 1% penicillin-streptomycin in a humidified atmosphere with 5% CO<sub>2</sub> at 37°C. The culture medium was removed every 72 hours. The culture medium was changed every 72 hours. The following experimental groups were formed:

GelMA-BT, GelMA-BT-GR1, GelMA-BT-GR1.5, and GelMA-BT-GR2:  $1.31 \times 10^3$  L929 cells were homogenized with 50  $\mu\text{L}$  of each hydrogel and placed in 96-well plates. They were then frozen for 1 hour at  $-30^\circ\text{C}$ ;

GelMA-BT-GR2<sup>#</sup>: 50  $\mu\text{L}$  of the hydrogel was placed in 96-well plates and frozen at  $-18^\circ\text{C}$  for 1 hour. Then  $1.31 \times 10^3$  L929 cells were added per well;

GelMA, GelMA/GR1, GelMA-GR1.5 e GelMA-GR2: 50  $\mu\text{L}$  of each hydrogel was homogenized with  $1.31 \times 10^3$  L929 cells and added to 96-well plates;

Positive control:  $1.31 \times 10^3$  L929 cells were added to 96-well plates without test materials;

Blank: wells containing only complete culture medium (without cells or test materials).

### MTT Assay

Cell viability was assessed using the MTT assay in triplicate at 24, 48, 72 and 168 hours following a protocol adapted from.<sup>14</sup> In brief, wells were rinsed with Dulbecco's phosphate-buffered saline (D-PBS) and 100  $\mu\text{L}$  of MTT solution (0.5 mg/mL) was added to each well. After 4 hours of incubation, the solution was removed and the formazan crystals were dissolved with 100  $\mu\text{L}$  dimethyl sulfoxide (DMSO). The absorbance was measured at 570 nm using a Biotek Elx 800 microplate reader.

### Statistical Analysis

Data were analyzed using GraphPad Prism 8<sup>®</sup>. Normality was determined by the Shapiro–Wilk test. A two-way ANOVA followed by Tukey's post-hoc test was performed. Results are presented as mean  $\pm$  standard deviation (SD), N=3, with significance defined at  $p < 0.05$ .

### CAM Assay

The ex egg chick chorioallantoic membrane (CAM) culture was conducted following established protocols from previous studies.<sup>15,16</sup> The eggshells were meticulously opened three days post-incubation to commence the ex egg culture. Cryoprinted scaffolds were implanted onto the chick embryo CAM on day seven. The samples were then incubated for an additional seven days before being harvested for imaging.

## Results and Discussion

### Bioink

#### Printability of the Hydrogel

First, we analyzed the injection performance (extrusion rating for 3D printing) of all tested formulations, as shown in [Figure 2F](#). This allows us to understand how the addition of graphene affects the ability of GelMA to be processed in 3D printing.

When comparing the results of GelMA with the formulations containing graphene ([Figure 2F](#)), we observed a general trend towards improved extrusion with the addition of graphene. This indicates that graphene plays a positive role in modifying the rheological properties of GelMA and facilitates the printing process. A dose-response relationship is

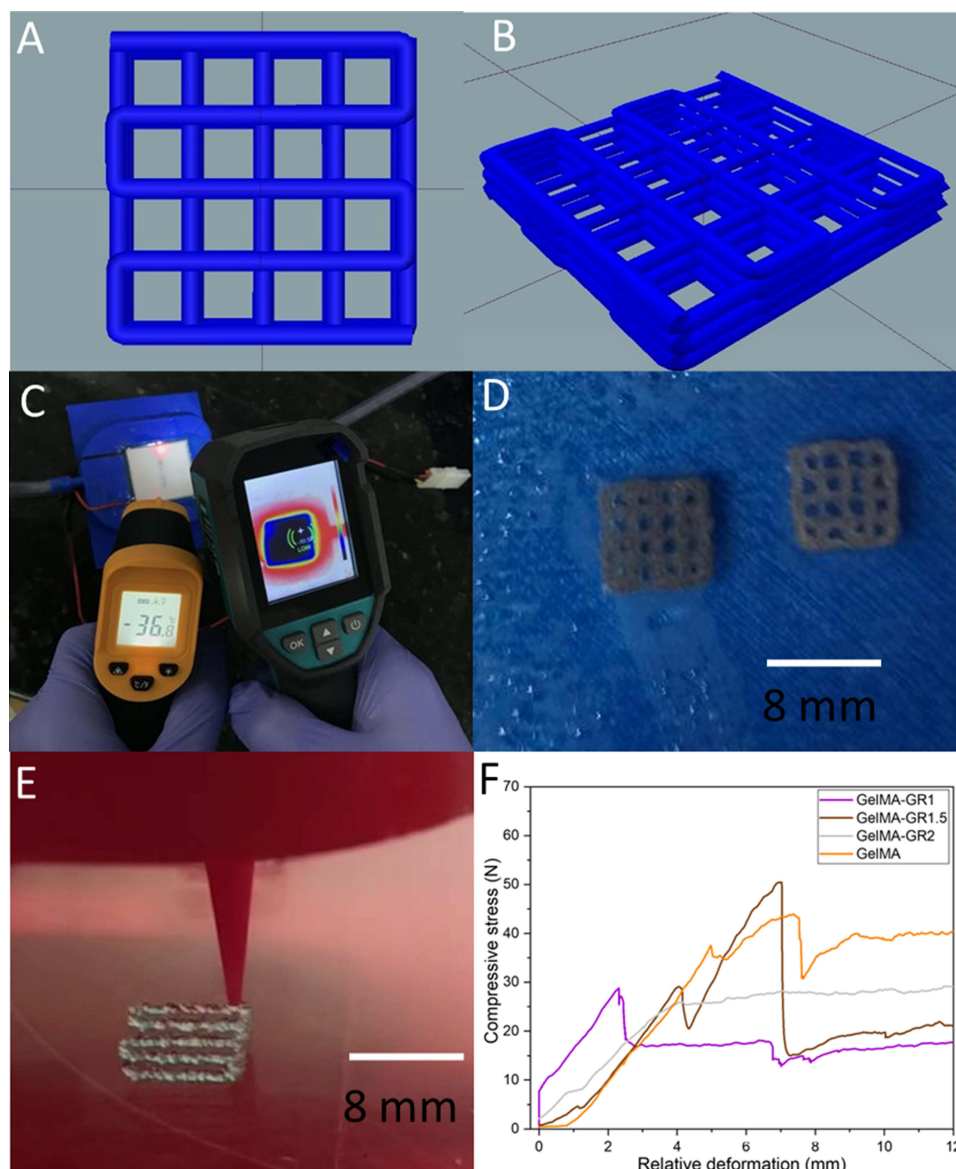


**Figure 2** Planning and Execution of 3D printing in different conditions: (A and B) Designed scaffold models, (C) temperature mapping of the low-temperature printing plate, (D) scaffolds after printing and (E) scaffolds during printing, and (F) Extrusion evaluation for 3D printing of the studied bioinks.

observed between graphene concentration and extrusion performance. The formulation with 2 mg/mL graphene (GelMA-GR2, in Figure 2) showed the best performance as it has a continuous N/mm curve, indicating that increasing the graphene concentration led to a significant improvement in the extrusion capability of the material.

One possibility is that the higher concentration of graphene led to a more intense interaction between the graphene particles and the GelMA matrix, resulting in better rheological stability and fluidity during the printing process. Additionally, it is important to consider the relationship between the viscosity of the material and the voltage applied during 3D bioprinting. Formulations with lower viscosity tend to require less tension to be extruded.<sup>17</sup> In this context, GelMA with 2 mg/mL of graphene presents an optimized viscosity that allowed a smoother and more controlled extrusion. This behavior was confirmed by the injectability test, which evaluated the force required to extrude each GelMA formulation in relation to the displacement of the syringe. It was observed that the formulation with 2 mg/mL of graphene showed the best performance, with a continuous N/mm curve, indicating that the higher concentration of graphene led to a significant improvement in the extrusion capacity of the material.

Thus, the results with GelMA and 2 mg/mL graphene are promising for several specific biomedical applications, such as the fabrication of scaffolds for tissue engineering, where precision and efficiency in cell deposition are crucial. Furthermore, this formulation can be used in the creation of complex biomimetic devices, such as heart valves and blood vessels, where uniformity and consistency in material extrusion are essential to the functionality of the device. Other applications include bioprinting tissue models for drug testing and disease studies, which require a detailed and reproducible structure for reliable results. Therefore, GelMA with 2 mg/mL of graphene proves to be an effective choice to advance 3D bioprinting on several fronts of biomedicine.

### Printability

GelMA and graphene scaffolds were successfully printed at room temperature and at low temperature. The scaffolds were designed as shown in Figure 2A and B, with the printed scaffolds in Figure 2D and E) showing the printed scaffolds. The low-temperature system was monitored during the printing of GelMA, as shown in Figure 2C, which shows the temperature zones and mapped areas determined with a thermometer.

### Structural Properties of the Hydrogel

Fourier transform infrared spectroscopy (FTIR) by has shown that GelMA has characteristic bands at 1244 and 1259  $\text{cm}^{-1}$  associated with the stretching vibrations of the C-N bond, as shown in Figure 3A. These results are confirmed by other studies showing that such bands are typical of amine groups. The band at 1548 and 1550  $\text{cm}^{-1}$  attributed to N-H bending vibrations is identified in materials containing amide groups as reported by.<sup>18</sup>

The band at 1643  $\text{cm}^{-1}$ , corresponding to C=O stretching vibrations, is characteristic of amide bonds in polymers such as GelMA. In addition observed that the band at 3293  $\text{cm}^{-1}$  is associated with N-H and O-H stretching vibrations, consistent with previous findings on the presence of hydroxyl and amino functional groups in biocompatible materials like GelMA.<sup>2</sup>

When analyzing the FTIR spectra of graphene-modified GelMA (GelMA/GR), as shown in Figure 3B, a shift and increase in the intensity of the identified bands was observed, suggesting a physical interaction between carboxygraphene and GelMA. The bands in the range of 3000 to 3600  $\text{cm}^{-1}$  indicate the presence of O-H bonds of the carboxyl group of graphene as well as hydrogen bonds between carboxygraphene and GelMA.<sup>19</sup> In addition, characteristic bands of graphene, such as the one observed at 1652  $\text{cm}^{-1}$ , can be attributed to the presence of aromatic C=C rings.

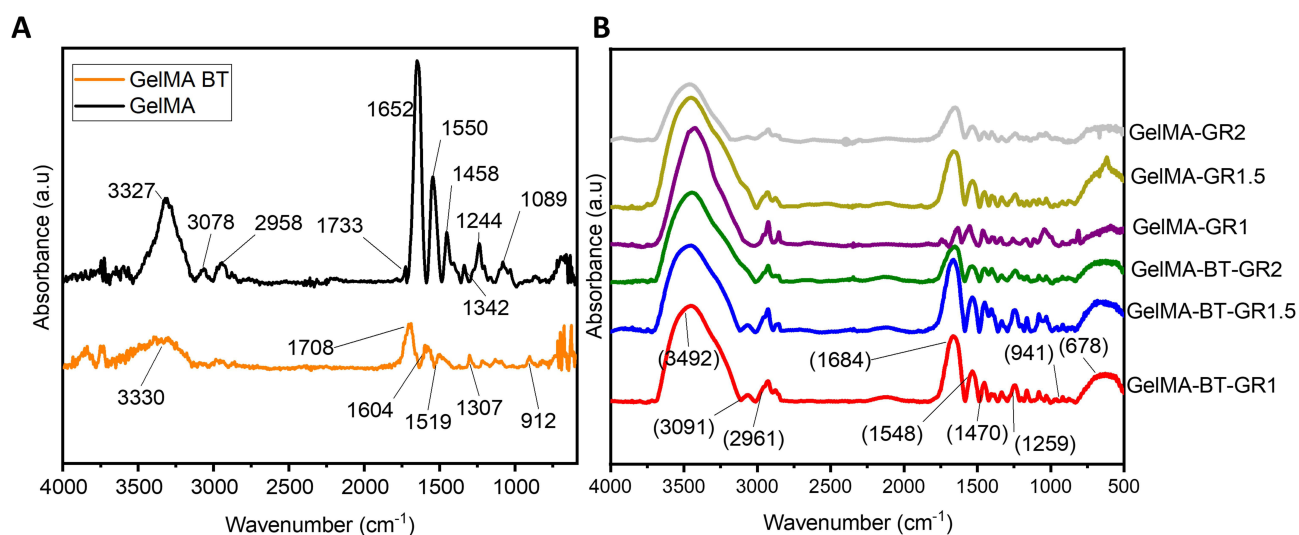


**Figure 3** Structural analysis of the material by Fourier Transform Infrared Spectroscopy (FTIR): **(A)** FTIR of GelMA and GelMA-BT. **(B)** FTIR of GelMA, GelMA/GR1, GelMA-GR1.5, GelMA-GR2, GelMA-BT, GelMA-BT-GR1, GelMA-BT-GR1.5 and GelMA-BT-GR2 bioinks.

It is important to note that the intensity of the bands at 3330 and 2958  $\text{cm}^{-1}$  compared to pure GelMA is due to evidence of C-H bonds.<sup>20</sup> Moreover, the range from 3500 to 3100  $\text{cm}^{-1}$  is related to the stretching of primary and secondary amines, which contributes to the characterization of the interactions in GelMA/GR.<sup>20,21</sup>

These results improve the understanding of the interaction between carboxygraphs and GelMA and provide a solid basis for the development of multifunctional biomedical materials with improved properties for various clinical applications. Comparison of the groups printed at room temperature and at low temperature shows that the material does not exhibit band shifts.

Differential Scanning Calorimetry (DSC) analysis, Figure 4, was used to investigate the effects of low temperature during the printing and crosslinking process of the material. The DSC of the hydrogels shows endothermic thermal transition events at around 100 °C, which can be attributed to the loss of free and bound water in the hydrogel.<sup>22</sup> In the hydrogels treated at low temperature, a thermal event can be observed at 200 °C, which may be related to material organization. This event is not observed in hydrogels crosslinked at room temperature, suggesting that the use of low temperatures leads to stronger chemical bonds.

This can be attributed to two factors: First, the state of the material at  $-30$  °C brings the molecules closer together, and when energy is provided via UV light for crosslinking, a larger number of bonds form due to this proximity. Second,

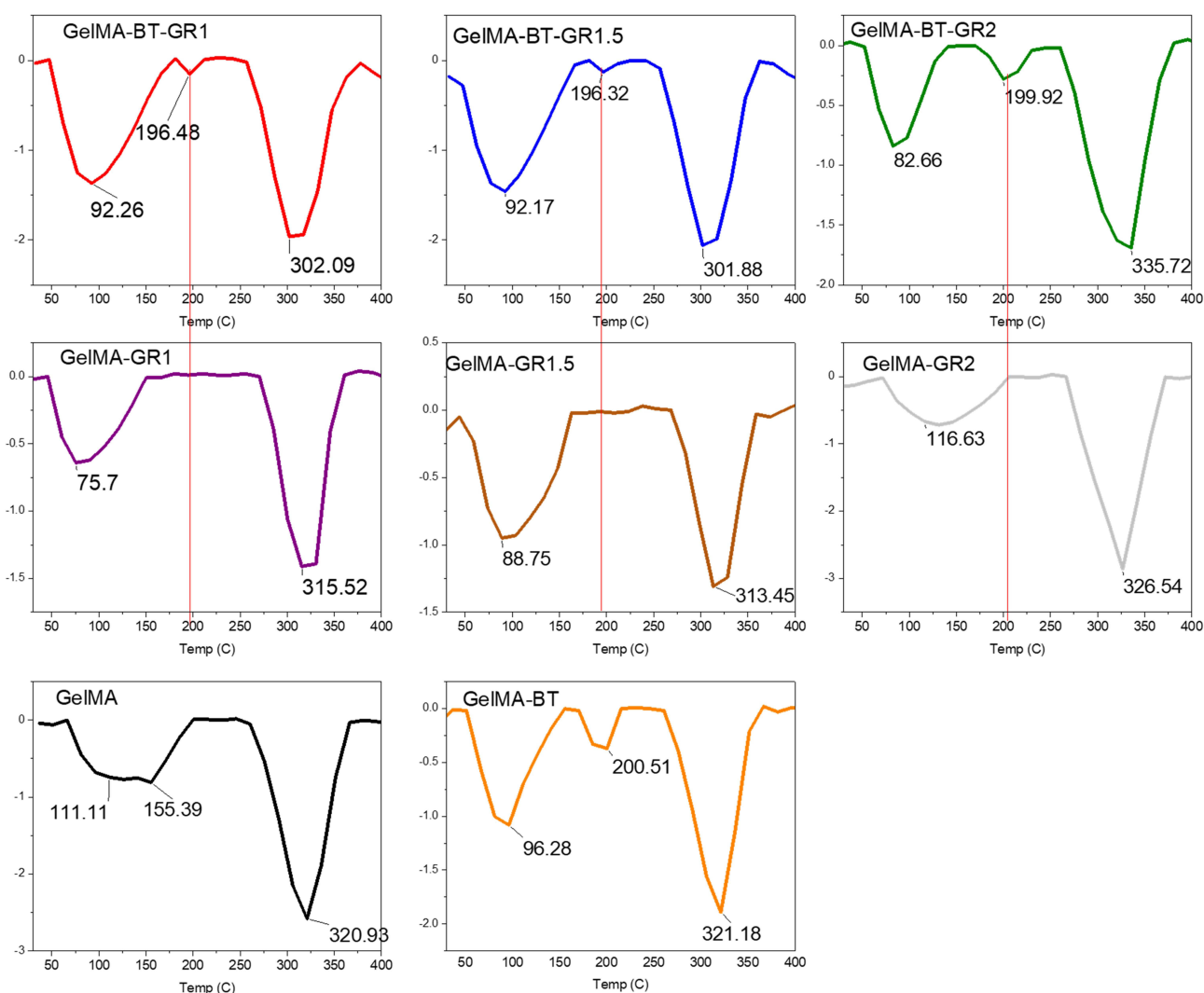


**Figure 4** Thermal characterization of the materials used by Differential Scanning Calorimetry (DSC) analysis of the bioinks: GelMA, GelMA/GR1, GelMA-GR1.5, GelMA-GR2, GelMA-BT, GelMA-BT-GR1, GelMA-BT-GR1.5 and GelMA-BT-GR2.

the water present in the hydrogel expands upon freezing, which presses against the hydrogel walls, making the material more compact. Under these conditions, crosslinking can result in the formation of a greater number of bonds. The third thermal event is related to the degradation of GelMA. This event is observed as a large endothermic transition associated with material degradation occurring between 250 and 400 °C.

Differential Scanning Calorimetry (DSC) analysis of the hydrogels revealed important information about the thermal events and the structural organization of the material. Table 2 shows the energy absorbed during these events, both in millijoules (mJ) and in joules per gram (J/g). With this data, we can point out advances and innovation in the work carried out.

The DSC results indicate the presence of three main thermal events. The first thermal event is related to the fusion of free water and the restructuring of the hydrogel. The low energy absorbed in this event suggests a minimal reorganization of the structure of GelMA-BT and GelMA-BT-GR2. Specifically, the absorbed energies were -178.52 mJ (-81.00 J/g) for GelMA-BT and -113.25 mJ (49.85 J/g) for GelMA-BT-GR2.

The second thermal event, observed at intermediate temperatures, is absent in GelMA samples without low-temperature crosslinking, indicating that crosslinking at -30°C promotes the formation of additional bonds. The absorbed energies for this event were 32.46 mJ (14.73 J/g) for GelMA-BT and 28.99 mJ (12.76 J/g) for GelMA-BT-GR2, suggesting that the proximity of molecules at this temperature favors the formation of a greater number of bonds when energy is supplied via UV light for cross-linking at low temperature.

The third thermal event is associated with the degradation of GelMA.<sup>23</sup> The absorbed energies were 283.81 mJ (128.77 J/g) for GelMA-BT and 332.55 mJ (146.37 J/g) for GelMA-BT-GR2, indicating greater thermal stability for the sample with graphene. This greater thermal stability can be attributed to the presence of graphene and low-temperature cross-linking, which together result in a more robust hydrogel network.

Current literature on nanocomposite hydrogels has shown that the incorporation of nanomaterials, such as graphene, can significantly improve the mechanical and thermal properties of hydrogels.<sup>23,24</sup> Thus, thermal analyzes indicated an improved interaction between the components, suggesting that the low temperature not only improves crosslinking, but also the integration of nanomaterials, optimizing the structural properties of the hydrogel.

The XRD pattern of the prepared hydrogels, as shown in Figure 5, reveals that the diffratogram of GelMA exhibits a broad peak at  $2\theta = 20.7^\circ$ , indicating the amorphous structure of the GelMA hydrogel.<sup>2</sup> This peak is also visible in all hydrogel nanocomposites, suggesting that graphene nanoplatelets were dispersed in the GelMA hydrogel network. This behavior is consistent with previous studies showing that the presence of graphene does not significantly alter the crystalline structure of GelMA due to its predominantly amorphous nature.<sup>20</sup> The literature suggests that cross-linking

**Table 2** Absorbed Energy in mJ (Millijoules) and J/g (Joules per Gram) During Thermal Events Inferred by Differential Scanning Calorimetry (DSC)

Events	1		2		3	
	mJ	J/g	mJ	J/g	mJ	J/g
GelMa	-194.78	-73.23	0	0	401.46	150.92
BT-GelMa	-178.52	-81.00	32.46	14.73	283.81	128.77
GelMa I	-129.88	-60.69	0	0	219.09	102.38
GelMa 1.5	-207.95	-84.53	0	0	194.33	79.00
GelMa 2	-158.74	-58.71	0	0	456.48	168.82
BT-GelMa I	-296.78	-125.33	7.36	3.11	369.90	155.21
BT-GelMa 1.5	-258.87	-100.30	6.74	2.61	346.00	134.06
BT-GelMa 2	-113.25	49.85	28.99	12.76	332.55	146.37



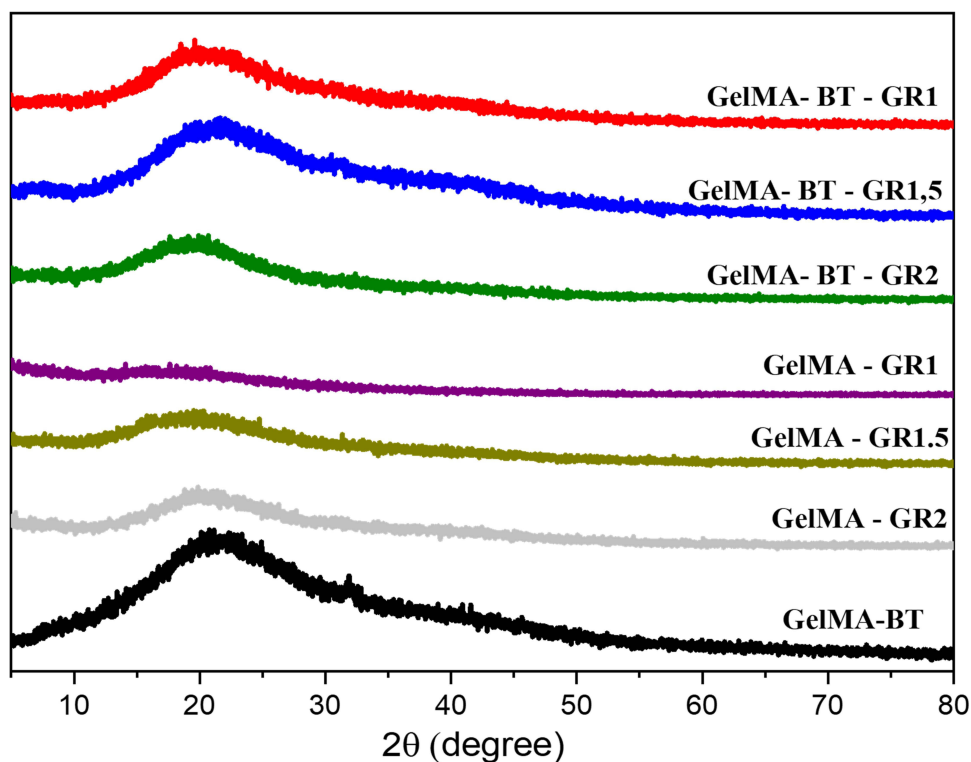


**Figure 5** X-ray diffraction (XRD) used to analyze the structural organization of GelMA-based bioinks with varying concentrations of graphene. The figure presents the XRD patterns of GelMA, GelMA/GR1, GelMA-GR1.5, GelMA-GR2, GelMA-BT, GelMA-BT-GR1, GelMA-BT-GR1.5 and GelMA-BT-GR2, demonstrating the effect of graphene on the internal structure of the hydrogel.

hydrogels at low temperatures can induce greater molecular organization, promoting crystallization, especially when the material structure is frozen before cross-linking.<sup>25–27</sup> This process can increase the proximity of molecules, facilitating the formation of a crystalline or semi-crystalline structure when energy is applied for cross-linking.

However, the XRD results showed a similar pattern between the nanocomposites and the pure GelMA hydrogel, without indicating the formation of crystallinity. This observation can be explained by several factors. Firstly, the amorphous nature of GelMA may have prevailed even under low temperature conditions, due to the intrinsic tendency of GelMA to maintain a disordered structure. Secondly, the physical interaction between the graphene nanoplatelets and the GelMA matrix may have restricted the mobility of the polymer chains, preventing the reorganization necessary for the formation of a crystalline structure.

However, cross-linking at low temperatures promoted better integration of the graphene nanoplatelets into the GelMA matrix, resulting in a more homogeneous distribution and a more cohesive material. Thermal analysis, such as DSC, indicated an enhanced interaction between the components, suggesting that the low temperature not only improves cross-linking, but also the integration of nanomaterials, optimizing the mechanical and structural properties of the hydrogel. Therefore, although the expected crystallization due to the effect of low temperature was not observed, the innovative approach of adding graphene and using low temperature for cross-linking provided hydrogels with improved mechanical properties and a more homogeneous structure.

The micrographs obtained by scanning electron microscopy (SEM), presented in Figure 6, reveal surfaces with interstitial spaces conducive to cell growth and proliferation, a desirable characteristic for tissue development. In Figure 7, the formation of pores is observed in the microscopic images of GelMA and GelMA-BT. GelMA-BT shows a greater amount of pore formation compared to GelMA, both on the surface (Figure 6a and d) and inside (Figure 6b,c, e and f). This difference can be attributed to the organization of the material during the printing and cross-linking processes, resulting in interconnected cavities that can facilitate cell proliferation and tissue formation.<sup>11</sup>



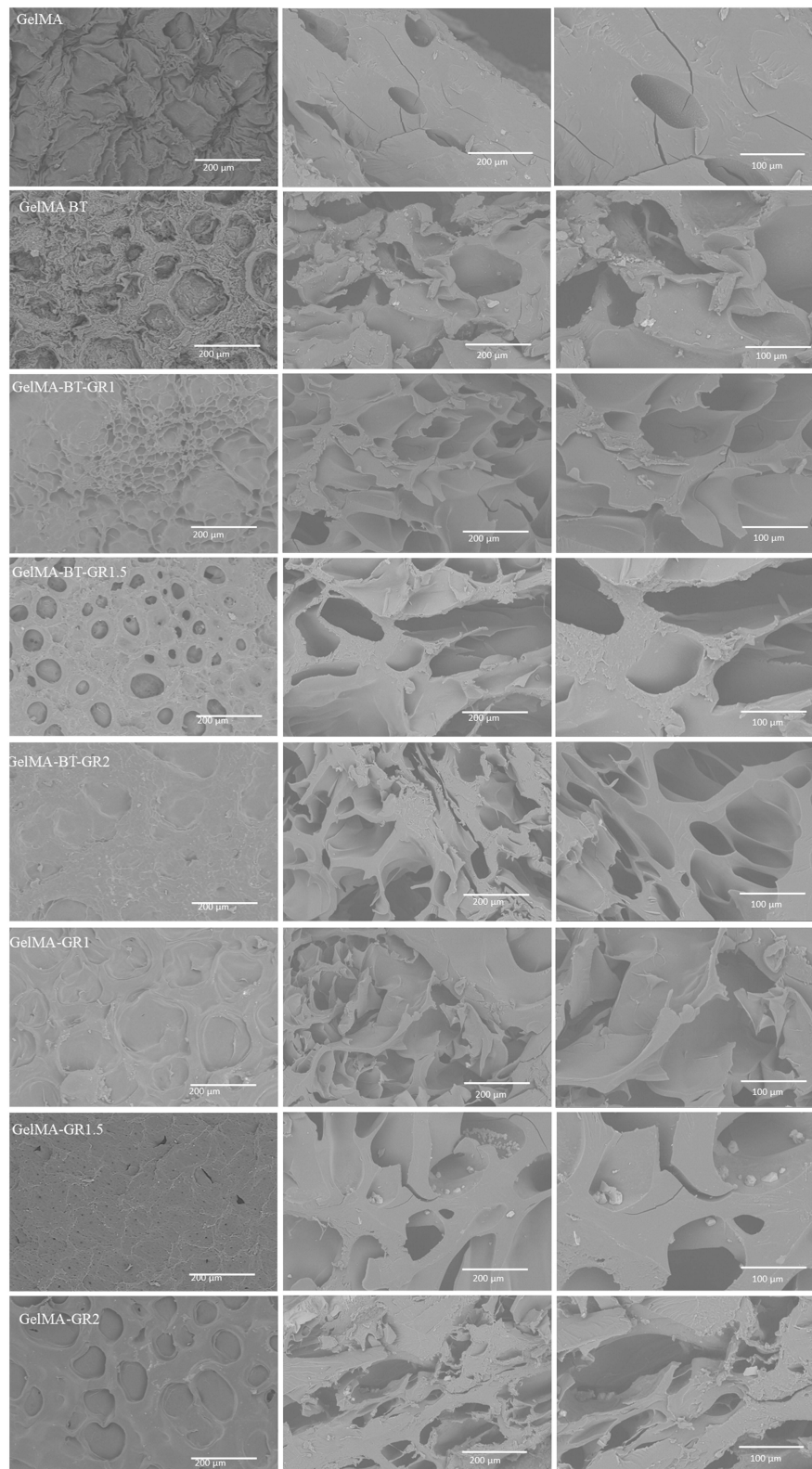


**Figure 6** Morphological Characterization by Scanning Electron Microscopy: Micrographs of the bioinks GelMA, GelMA/GR1, GelMA-GR1.5, GelMA-GR2, GelMA-BT, GelMA-BT-GR1, GelMA-BT-GR1.5 and GelMA-BT-GR2.

This pattern is repeated in structures with the addition of graphene, as reported in the literature, where the increase in graphene results in a greater number of pores.<sup>2</sup> However, more regular void formation is observed at low temperatures than when printed at room temperature. Furthermore, cracks can be observed in the cross section of the scaffolds printed at room temperature, indicating a more fragile material compared to those printed at low temperature. This difference can be attributed to the better adhesion of graphene to GelMA and the greater compaction due to the presence of water in the structure.

DSC results corroborate these observations, demonstrating that GelMA-BT scaffolds exhibit different thermal transitions compared to GelMA. Thermal analyzes show greater thermal stability and different phase transition behaviors in graphene-containing scaffolds, especially those printed at low temperatures. Crosslinking at low temperatures can provide greater thermal resistance and better structural organization, which can contribute to less crack formation and greater regularity of pores observed in SEM images.<sup>11,12</sup>

The area of these pores can be measured with the ImageJ software. **Figure 7A-H)** shows the microscopic images of the cross-section of each group and **Figure 7I** shows the area of these pores. In the black and white micrographs, the porosity, highlighted by the black coloration, can be seen, with GelMA having a lower porosity than GelMA-BT. This makes the printing and treatment of GelMA at low temperature quite interesting if the goal is to increase porosity for cell growth.<sup>12</sup>

As can be seen in **Figure 7**, GelMA combined with graphene at different concentrations presents larger pore areas than GelMA. The addition of graphene to GelMA can lead to increased porosity in the final material for several reasons, including particle distribution, volume increase, nucleation effect, and the interaction between the matrix and particles.<sup>2,20,28</sup>

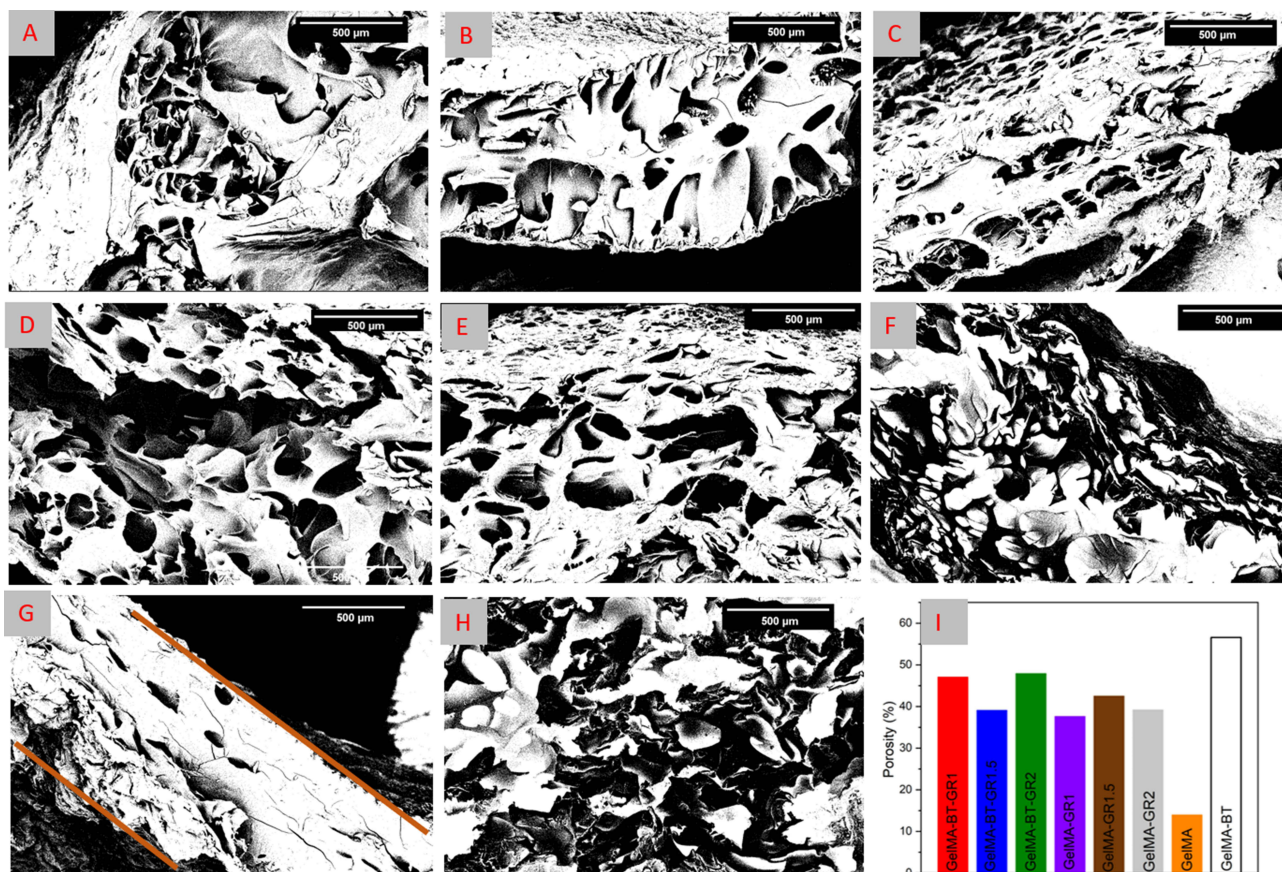


**Figure 7** The pore area measured using the image J software in the SEM micrographs of the bioinks (A) GelMA/GRI, (B) GelMA-GRI.5, (C) GelMA-GR2, (D) GelMA-BT-GR1, (E) GelMA-BT-GR1.5, (F) GelMA-BT-GR2, (G) GelMA, (H) GelMA-BT and (I) Porosity (%).

In particle distribution, graphene, when added to GelMA, can change the distribution of particles in the composite material.<sup>29</sup> Depending on the preparation method and graphene concentration, graphene particles may disperse more evenly in the GelMA matrix. This more uniform dispersion can lead to the formation of interstitial spaces or porosity between particles, increasing the overall porosity of the material.<sup>29,30</sup> The increase in volume may be due to the fact that graphene has a large surface area and a two-dimensional structure, which can increase the volume of the composite material when incorporated into GelMA.<sup>30</sup> This can result in the formation of pores during the gelation or cross-linking phase of GelMA, when graphene interacts with the polymer matrix and integrates into the material's three-dimensional structure.<sup>30,31</sup>

Due to the nucleation effect, graphene can act as nucleation centers during the GelMA solidification process. This means that graphene particles can promote the formation of new phases or structures during solidification, leading to the formation of pores in the matrix. Depending on the surface properties and the compatibility between GelMA and graphene, phase separation or agglomeration of graphene particles may occur, resulting in areas of greater porosity in the matrix.<sup>1,3</sup>

When comparing these values in Figure 7I with the literature, we found that the addition of graphene to GelMA tends to increase the porosity of the material, corroborating previous studies.<sup>1,20</sup> In studies by<sup>32</sup> observed that the incorporation of graphene into GelMA hydrogels resulted in a significant increase in porosity due to the interaction between the graphene nanoparticles and the GelMA matrix, facilitating the formation of pores during gelation and cross-linking. In the study by et al,<sup>33,34</sup> the addition of graphene to GelMA hydrogels increased the porosity from 15% to about 45%, depending on the graphene concentration, which is consistent with the results presented in Figure 7I of the present study, where the porosity varies between approximately 37% to 47% with different graphene concentrations.

Figure 7I shows that the group with the highest porosity containing graphene is GelMA-BT-GR2, highlighting the influence of a higher concentration of graphene and low temperature in this material. This is interesting for use as a biomaterial, as greater porosity can allow better cell growth. Furthermore, it is observed that materials with a higher concentration of graphene, such as GelMA-BT-GR2, have increased thermal stability. This stability can be attributed to the presence of graphene, which improves heat dissipation and reinforces the material's structure.

And the greater porosity, although beneficial for cell growth, can negatively affect the mechanical resistance of the material. However, graphene scaffolds, especially those with higher concentration, present an optimized combination of porosity and mechanical strength. Graphene acts as a reinforcement within the GelMA matrix, improving discomfort and fracture resistance, as indicated by stress-strain analyses. This mechanical improvement, together with the high porosity and thermal stability, makes GelMA-BT-GR2 a candidate for tissue engineering applications.

## Mechanical Properties of Hydrogels

Graphene is known for its high mechanical strength and rigidity. When graphene is added to GelMA in increasing concentrations, it acts as a reinforcing agent, strengthening the GelMA matrix and improving its mechanical properties.<sup>7,19,34</sup> The presence of more graphene particles in the matrix can result in a more robust network that can withstand greater compressive forces. At higher graphene concentrations, the dispersion and distribution of the graphene particles in the GelMA matrix can be more uniform. This can lead to a more homogeneous load distribution throughout the material structure, resulting in a more uniform compressive resistance throughout the sample. This is consistent with the increasing compressive strength values observed with added graphene, Figure 8A: GelMA-GR1 exhibited a stress of 19 KPa, GelMA-GR1.5 a stress of 23 KPa and GelMA-GR2 a stress of 24 KPa. The interaction between graphene particles and the GelMA matrix also plays an important role in the compressive strength of the composite material. At higher graphene concentrations, there can be a stronger interaction between the graphene particles and the polymer matrix, resulting in a more cohesive and resistant network.<sup>34</sup>

In compression with graphene scaffolds fabricated at low temperature, the mechanical compressive strength values of the GelMA-BT groups were significantly higher. GelMA-BT showed a stress of 27 KPa, GelMA-BT-GR1 a stress of 36 KPa, GelMA-BT-GR1.5 a stress of 32 KPa and GelMA-BT-GR2, one of the best groups in this study, showed a stress of 31 KPa. These values are significantly higher compared to GelMA-GR2. In percentages, the evolution resistance values of the groups GelMA-BT (27 kPa), GelMA-BT-GR1 (36 kPa), GelMA-BT-GR1.5 (32 kPa) and GelMA-BT-GR2 (31



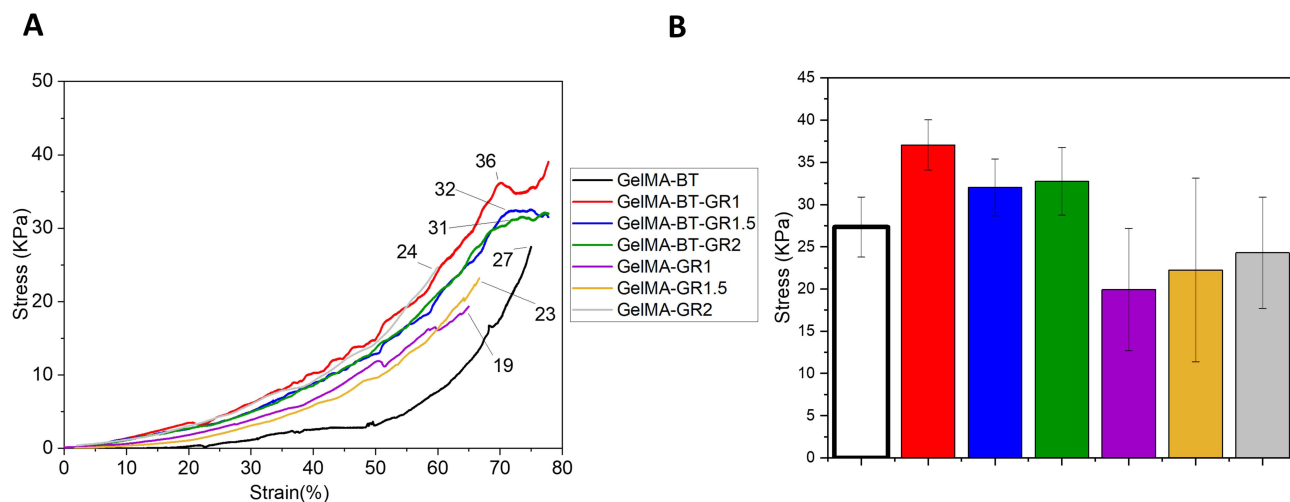


**Figure 8** Mechanical analysis of the scaffolds: **(A)** Stress-strain graph of compressive strength of the scaffolds GelMA-GR1, GelMA-GR1.5, GelMA-GR2, GelMA-BT, GelMA-BT-GR1, GelMA-BT-GR1.5 and GelMA-BT-GR2. **(B)** Graph of maximum compressive strength and standard deviation. Data are expressed as mean  $\pm$  SD, N = 3, one-way ANOVA, Tukey's Test,  $p < 0.01$ .

kPa) were significantly higher than the values for cross-linked scaffolds at room temperature. Comparing GelMA-GR2 (24 kPa) with GelMA-BT-GR2 (31 kPa), we observed an approximately 29% increase in specification strength due to low temperature processing. Similarly, GelMA-BT-GR1 showed an 89% increase compared to GelMA-GR1.

The difference in compressive strength between the GelMA with graphene scaffolds fabricated at room temperature and those fabricated at low temperatures can be attributed to factors such as the effect of temperature on the material structure, increased cross-linking, improved integration of graphene into the matrix and improved dimensional stability. These results are consistent with the thermal events observed in the DSC and the microscopic images, which show higher porosity and thus better densification.

A low temperature during the production process can influence the molecular structure and organization of the graphene particles in the GelMA matrix.<sup>12</sup> This can lead to a more compact and cohesive structure in the scaffolds produced at low temperatures, which contributes to higher compressive strength, as observed in GelMA-BT-GR2. In addition, low temperature can promote more effective crosslinking of GelMA, resulting in a stronger and more resistant molecular network. Cross-linking is the process by which GelMA molecules are linked together to form a stable three-dimensional structure.

Better integration of graphene particles into the GelMA matrix can be achieved by a more uniform distribution of graphene particles or a more effective interaction between graphene and GelMA molecules. As a result, scaffolds produced at low temperatures may exhibit higher compressive strength due to the reinforcement provided by graphene.

Improved dimensional stability can also be achieved through the use of low temperatures, as these can help maintain dimensional stability during scaffold fabrication, resulting in more uniform and consistent structures. This can contribute to a more homogeneous distribution of mechanical properties, including compressive strength, in frameworks produced at low temperatures.

In the present study, it was observed that the group with GelMA at the concentrations used did not present adequate mechanical properties to carry out the mechanical tests.

The analysis of **Figure 8B** reveals that, although there were no statistically significant differences between the compressive strength of scaffolds produced at low temperature compared to those fabricated at room temperature, an important trend was observed. The groups processed at low temperature exhibited lower standard deviations in their maximum compressive strength values. This suggests a more consistent mechanical performance within these groups. The reduced variation in compressive strength indicates that the scaffolds fabricated at low temperatures may benefit from a more uniform structural organization, potentially due to improved integration of graphene into the GelMA matrix.

As a result, the mechanical properties in these groups appear to be more homogeneous, contributing to more predictable performance under compressive loads.

## Toxicity

The test was performed between 24 and 48 hours (Figure 9) to check the toxicity of the GelMA/GR bioink as it elicits biomonitoring and pharmacological results.<sup>35</sup> In this regard, the tested material was not toxic to *A. salina*. The result is illustrated by Figure 10, which shows the percentage of surviving nauplii at concentrations of 0.1–5 mg/mL. In addition, it shows the results in significant form, indicating an average survival rate of 90%, which means that the material has low toxicity and low variability of results.

The non-toxicity of the GelMA, GelMA-GR1, GelMA-GR1.5, GelMA-GR2, GelMA-BT, GelMA-BT-GR1, GelMA-BT-GR1.5 and GelMA-BT-GR2 groups, as demonstrated by the nauplii survival test (Figure 9) at various concentrations, is an encouraging result for tissue engineering and other biomedical applications. The proven safety of the materials in survival tests on living organisms suggests that they may be suitable for in vivo use in animal models and eventually for clinical applications. This opens up possibilities for the development of implants and biomedical devices based on GelMA-GR-BT for tissue regeneration and organ repair.

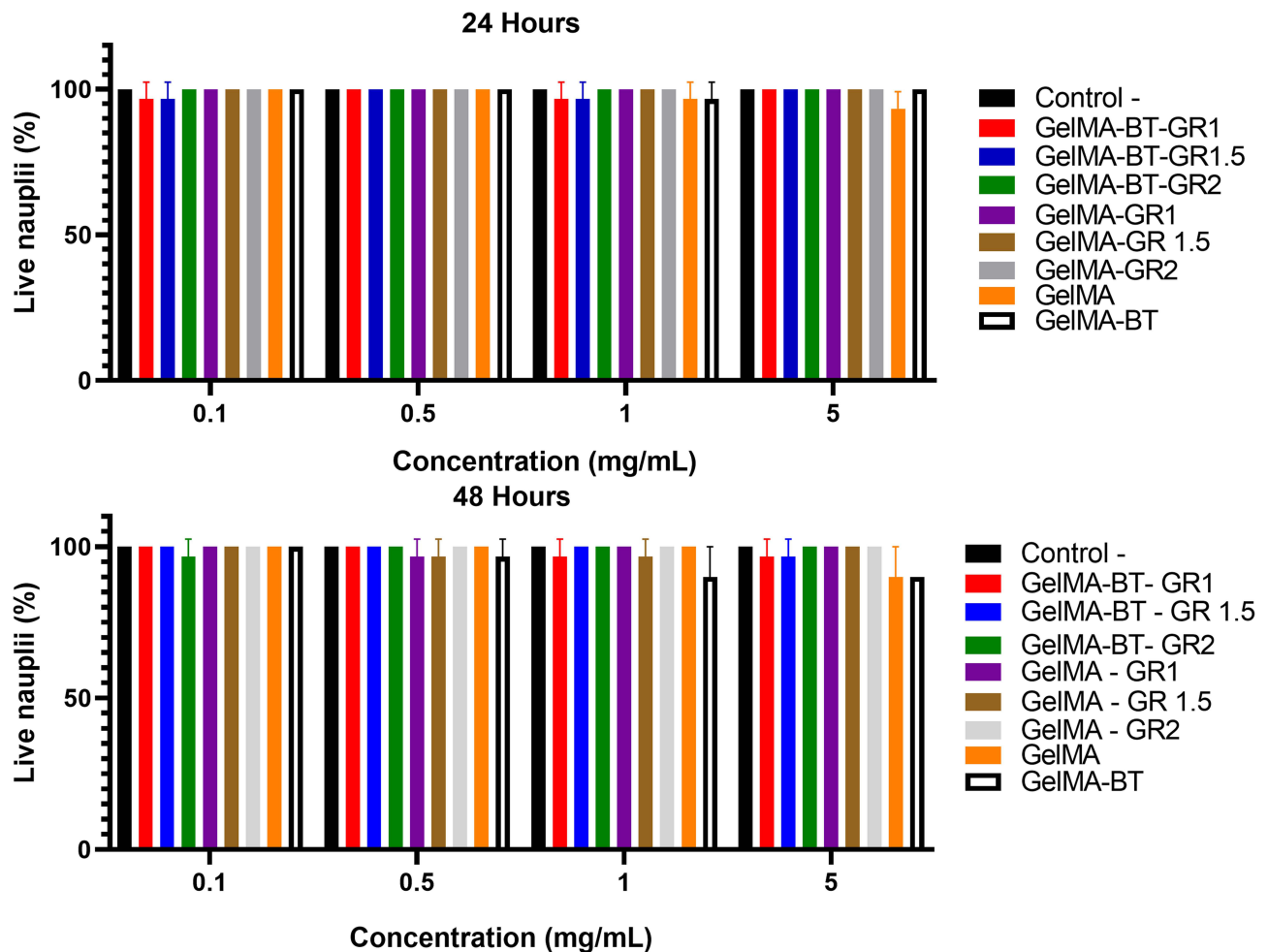


**Figure 9** Toxicity analysis: Survival of nauplii at concentrations of 0.1–5 mg/mL in 24 and 48 hours for the groups: GelMA, GelMA-GR1, GelMA-GR1.5, GelMA-GR2, GelMA-BT, GelMA-BT-GR1, GelMA-BT-GR1.5 and GelMA-BT-GR2. Data are expressed as mean  $\pm$  SD, N = 3, one-way ANOVA, Tukey's Test,  $p < 0.05$ .

## Cytotoxicity Evaluation of GelMA and Graphene-Based Hydrogels in L929 Cells

The MTT assay showed significant effects of treatment, time and their interaction on cell viability ( $p < 0.05$ ) (Figure 10). After 24 hours, absorption was similar in all groups, probably due to insufficient time for cell adhesion and proliferation. At 48 hours, GelMA, GelMA-GR1 and GelMA-GR1.5 showed higher absorption, which was not significantly different from the control, while GelMA-BT, GelMA-BT-GR1, GelMA-BT-GR1.5 and GelMA-BT-GR2 showed significantly lower absorption ( $p < 0.05$ ).

This pattern continued after 72 hours, apart from GelMA-GR1.5 (significant decrease,  $p < 0.05$ ) and GelMA-GR2, which showed a strong increase compared to 48 hours and reached similar values as the control. The GelMA group showed the highest absorption, followed by GelMA-GR2, which did not differ from the control group. After 168 hours, GelMA-BT, GelMA-BT-GR1, GelMA-BT-GR1.5, GelMA-BT-GR2 and GelMA-GR1 showed absorption close to zero,

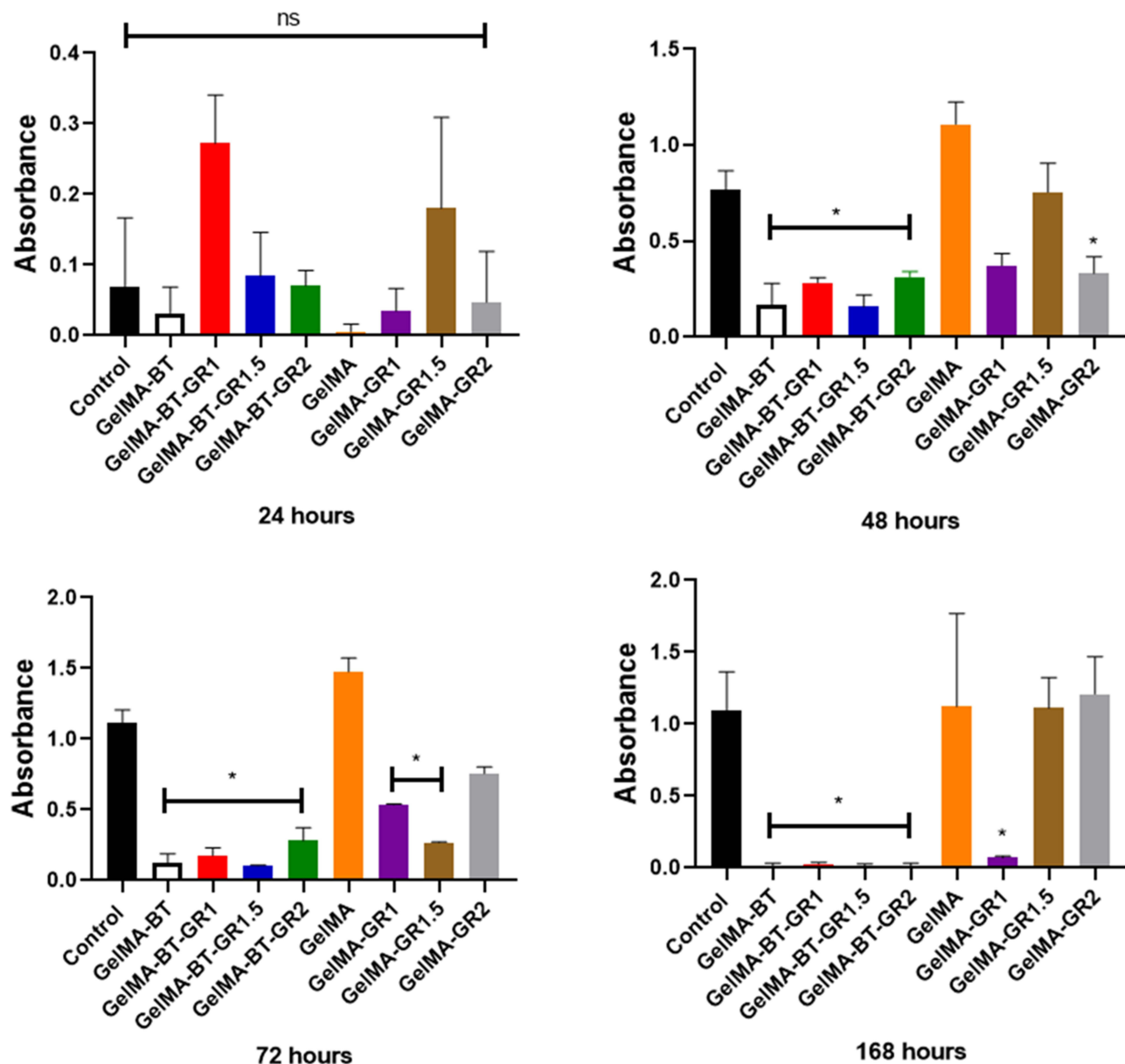


**Figure 10** Cytotoxicity of GelMA, GelMA-GR1, GelMA-GR1.5, GelMA-GR2, GelMA-BT, GelMA-BT-GR1, GelMA-BT-GR1.5, and GelMA-BT-GR2 hydrogels in L929 murine fibroblasts evaluated by the MTT assay. Absorbance at 570 nm, indicative of cell viability, was measured at 24, 48, 72, and 168 hours after treatment. The data are presented as mean absorbance values for each hydrogel and the control. Data are expressed as mean  $\pm$  SD, N = 3, two-way ANOVA, Tukey's multiple comparisons test, (\*)  $p < 0.05$ , ns = not significant mean statistical differences.



indicating cell death. GelMA and GelMA-GR1.5 showed similar values, with GelMA-GR1.5 showing an increase, indicating possible cell recovery or degradation of the treatment due to changes in the culture medium. Of note, GelMA, GelMA-GR1.5 and GelMA-GR2 showed no significant difference compared to the control throughout the study, indicating minimal cytotoxic effects.

Studies show that high concentrations of non-functionalized graphene can induce inflammatory reactions and cytotoxicity.<sup>36</sup> But, low-temperature printing could be crucial for incorporating high graphene contents into GelMA, ensuring the formation of scaffolds with superior mechanical properties without compromising cellular proliferation.

To compare the effect of low temperatures on the material, one of the best groups, GelMA-GR2, was selected, which was produced in three different systems: GelMA-GR2, in which the cells were mixed at 37°C and the material was then crosslinked; GelMA-BT-GR2, in which the cells were mixed at 37°C and the material was then frozen at -30°C for 1 hour to simulate low temperature printing and then crosslinked; and GelMA-BT-GR2#, in which the material was frozen at -30°C for 1 hour to simulate low temperature printing, then crosslinked, and then the cells were added at 37°C.

After these processes, the culture medium was added and the materials were incubated in a cell culture incubator for different periods of time: 24h, 48h, 72h and 168h. The results showed that the GelMA-BT-GR2 system exhibited low cell viability over time (Figure 11). On the other hand, the GelMA-GR2 and GelMA-BT-GR2# systems showed excellent and superior cell viability compared to the control, with the GelMA-BT-GR2# group showing the best cell viability of all groups, including the control, after 168h. These results suggest that by developing a non-toxic cryopreservative for the cells, it will be possible to perform bioprinting at low temperatures.<sup>12</sup> Although low temperature printing has shown better mechanical properties, the cells should be added after the printing process to ensure cell viability. Like this the integration of graphene into GelMA hydrogels, combined with low-temperature printing, presents an innovative and promising approach for fabricating advanced scaffolds for tissue engineering. These materials not only improve mechanical and biological properties, but also prove to be safe for biomedical applications, in line with recent advances in the literature.<sup>7,36</sup>

## CAM Assay

The CAM assay was employed to evaluate the angiogenic potential of the cryoprinted scaffolds. The cryoprinted constructs were implanted on day 7 of the ex egg CAM and were collected after an additional 7 days of incubation (Figure 12A). To quantify the angiogenic response around the different cryoprinted constructs, the average lengths of newly formed blood vessels were measured. As shown in Figure 12B, the shortest average blood vessels length was observed in the control group (ie, eggs without material), whereas the inclusion of GelMA-BT-GR2 resulted in a significant increase in blood vessels length. The GelMA-BT-GR2 cryoprinted construct facilitated enhanced vascular growth, indicating that the GelMA and graphene cryoprinting process did not impair the functionality of vascular endothelial growth factor.

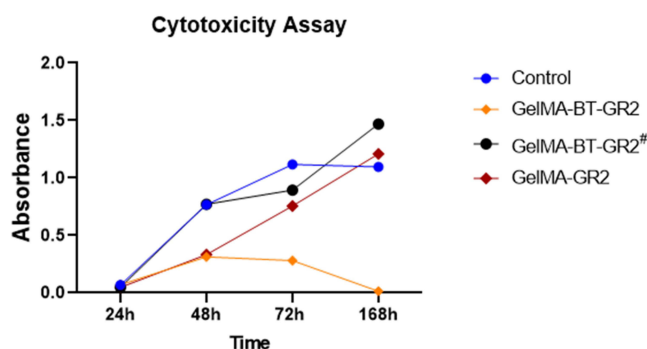


**Figure 11** Cytotoxicity of GelMA-GR2, GelMA-BT-GR2 e GelMA-BT-GR2# hydrogels in L929 murine fibroblasts evaluated by the MTT assay. Absorbance at 570 nm, indicative of cell viability, was measured at 24, 48, 72, and 168 hours after treatment. The data are presented as mean absorbance values for each hydrogel and the control group (cells without hydrogel treatment). Data are expressed as mean  $\pm$  SD, N = 3, two-way ANOVA, Tukey's multiple comparisons test,  $p < 0.05$ .

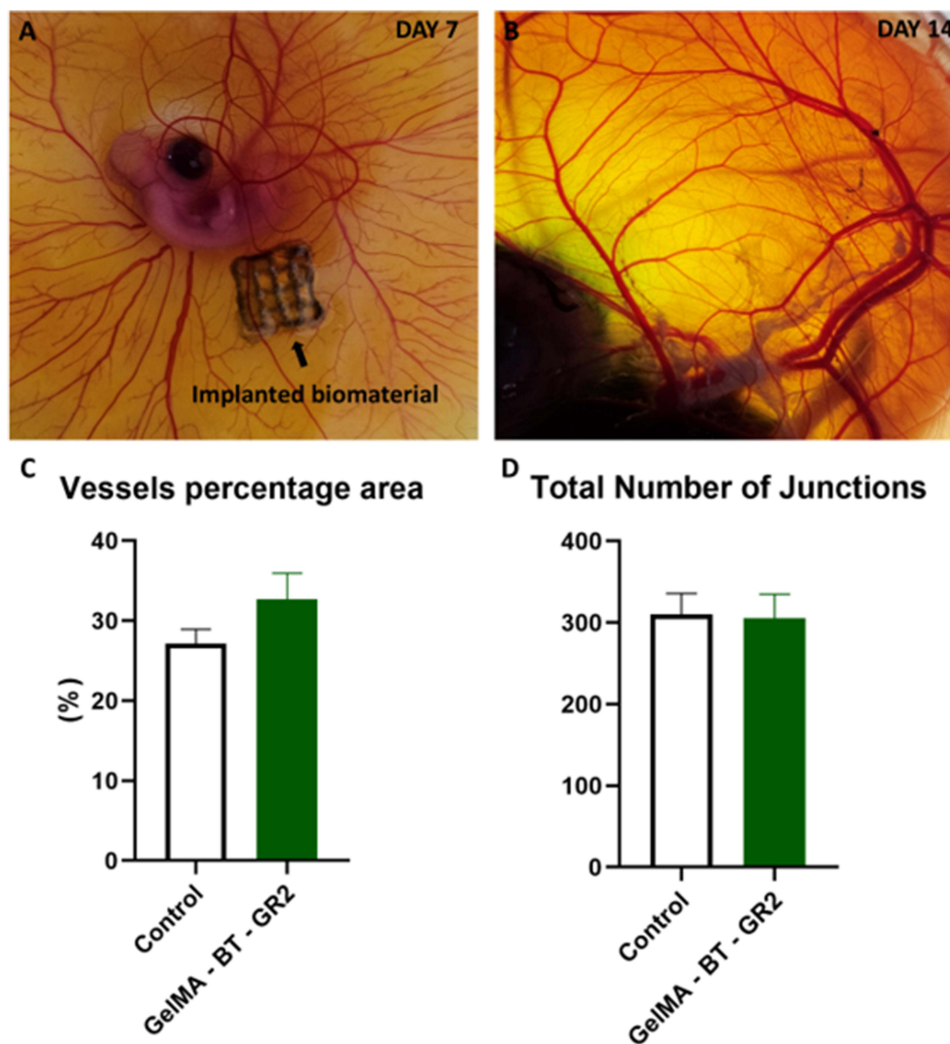


**Figure 12** Chick ex egg culture and CAM assay for investigating the vascularization in cryoprinted scaffolds. (a and b) Representative images of chick ex egg culture with implanted cryoprinted scaffolds for CAM assay. (c and d) Quantification of the blood vessels growth surrounding and within the cryobioprinted constructs by measuring different parameters: (c), Vessels percentage area, (d), Total Number of Junctions. Error bars indicate standard deviations. A two-tailed Student's *t*-test was used to find the *p* values. *n* = 5.

Almost no BVs grew into the control group, while the vascular infiltration in the GelMA-BT-GR2 group was higher. Furthermore, the GelMA-BT-GR2 group exhibited a higher percentage area of blood vessels compared to the control group (Figure 12C). This indicates enhanced angiogenesis in the presence of GelMA-BT-GR2. Additionally, the total number of vessel junctions in the GelMA-BT-GR2 group was comparable to that of the control group (Figure 12D), suggesting that the GelMA-BT-GR2 construct does not exhibit cytotoxic effects. These findings underscore the potential of GelMA-BT-GR2 as a promising material for promoting vascularization without compromising cellular viability. These *in vitro* cell Cytotoxicity evaluation and ex egg CAM assays highlight the effectiveness of the cryoprinting technique as a viable method for producing cell-laden implants or tissue models.

Table 3 compares the effectiveness of the low temperature printed GelMA-GR2 system (GelMA-BT-GR2) in terms of compressive strength with other similar systems described in the literature. This study showed that GelMA-BT-GR2 achieved a compressive strength of 31 kPa, significantly outperforming compressive strength values reported in previous studies for GelMA composites with other substances.

Previous studies indicate that the compressive strength of GelMA composites with different graphene concentrations varies between 20 kPa and 180 kPa, depending on the concentration and type of graphene used. In comparison, GelMA-

**Table 3** Comparison of Some Properties of This Work with Studies Reported in the Literature

Literature Works	Compression Resistance	MTT	References
Gelma High and Graphene in different concentrations	GelMA = 20 kPa; Gel 0.25G = 100 kPa Gel 0.50G = 180 kPa; Gel 0.75G = 80 kPa Gel 1 G = 60 kPa	0.5% GO Viable 1% GO No test	[2]
GelMA/HAMA-MXene	GelMA = 16.75 kPa; GelMA/HAMA = 17.40 kPa GelMA-MXene = 26.76 kPa; GelMA/HAMA-MXene = 27.46 kPa	Viable	[1]
GelMA/alginate/PEGDMA/xanthan gum	17–360 kPa	Viable	[37]
GelMA and Graphene	GelMA-BT= 27 KPa GelMA-BT-GR2 = 31 KPa GelMA-GR2 = 24 MPa	2 mg/mL GR Viable	<b>This work</b>

BT-GR2 in this study showed competitive performance with a resistance of 31 kPa, highlighting the effectiveness of the low-temperature method in improving the mechanical properties of the material.<sup>2</sup>

For GelMA composites with HAMA and MXene, the compressive strength ranges from 16.75 kPa to 27.46 kPa. The value obtained in this study for GelMA-BT-GR2 (31 kPa) is higher, suggesting that the combination of GelMA and graphene can result in a more robust structure, especially under low temperature conditions.

This study presents a wide range of compressive strengths (17–360 kPa), depending on the specific formulation. However, higher values are generally achieved with more complex formulations.<sup>1</sup> GelMA-BT-GR2's 31 kPa resistance, although not at the top of this range, is notable for a less complex system.

In Table 3, printing at low temperatures significantly improves the mechanical properties of GelMA-GR2 scaffolds. The increased compressive strength of GelMA-BT-GR2 compared to many systems described in the literature suggests that the low-temperature technique is a promising approach for developing biocompatible materials with improved mechanical performance. These results suggest potential for advanced biomedical applications, including bioprinting and tissue regeneration, where mechanical strength and cell viability are critical. In this work, GelMA-BT-GR2 uses the highest concentration of graphene and showed cell viability similar to the control, standing out among other studies for combining a high concentration of graphene with good mechanical properties, despite the lower concentration of the GelMA matrix.

## Conclusion

In this study, we successfully developed and characterized low-temperature 3D-printed GelMA/graphene bioinks, showing significant improvements in mechanical properties and scaffold stability. The compressive strength of the scaffolds increased with the addition of graphene, with GelMA-GR2 achieving a stress of 24 kPa and GelMA-BT-GR2 reaching 31 kPa, representing a 29% improvement due to low-temperature processing. Furthermore, differential scanning calorimetry (DSC) indicated enhanced thermal stability, with the energy absorbed during degradation being higher in scaffolds containing graphene.

The structural integrity of the scaffolds, confirmed by SEM analysis, demonstrated an increase in porosity with higher graphene concentrations, ranging from 37% to 47%. These properties make the GelMA/graphene bioinks promising candidates for applications in tissue engineering, where mechanical strength and porosity are crucial for scaffold performance. The resultant GelMA/graphene scaffolds exhibit superior mechanical properties, biocompatibility, and the ability to promote vascularization, making them highly suitable for various tissue engineering and regenerative medicine applications. Future studies should focus on further optimizing graphene functionalization and investigating long-term in vivo performance to fully harness the therapeutic potential of these advanced biomaterials.

## Funding

A.O.L thank to CNPq (403890/2023-3 and 310883/2020-2). F.R.M. thank to CNPq (311531/2020-2).

## Disclosure

The authors report no conflicts of interest in this work.

## References

1. Li J, Moeinzadeh S, Kim C, et al. Development and systematic characterization of GelMA/alginate/PEGDMA/xanthan gum hydrogel bioink system for extrusion bioprinting. *Biomaterials*. 2023;293:121969. doi:10.1016/j.biomaterials.2022.121969
2. Najjarzadegan M, Nouri Khorasani S, Khalili S, et al. A new shear-thinning nanocomposite hydrogel from GelMA-GO for soft tissue engineering. *Eur Polym J*. 2023;195:112204. doi:10.1016/j.eurpolymj.2023.112204
3. e Silva MDSC, de Sousa GF, Das Virgens Santana M, Tsumura WG, Stocco TD, Lobo AO. Tailoring mechanical properties of bioprinted GelMA scaffolds with multilayers of PLA/laponite nanocomposite fibers. *Mater Lett*. 2024;364:136314. doi:10.1016/j.matlet.2024.136314
4. Olate-Moya F, Arens L, Wilhelm M, Mateos-Timoneda MA, Engel E, Palza H. Chondroinductive alginate-based hydrogels having graphene oxide for 3D printed scaffold fabrication. *ACS Appl Mater Interfaces*. 2020;12(4):4343–4357. doi:10.1021/acsami.9b22062
5. Kang MS, Kang JI, Le Thi P, et al. Three-dimensional printable gelatin hydrogels incorporating graphene oxide to enable spontaneous myogenic differentiation. *ACS Macro Lett*. 2021;10(4):426–432. doi:10.1021/acsmacrolett.0c00845
6. Nazar V, Kashi M, Haghbin nazarpak M, Shahryari E, Mehrjoo M. Gelatin hydrogel reinforced by graphene oxide grafted chitosan for cartilage tissue engineering application. *Int J Polym Mater Polym Biomater*. 2023;72(14):1120–1131. doi:10.1080/00914037.2022.2085704
7. Bitounis D, Ali-Boucetta H, Hong BH, Min D, Kostarelos K. Prospects and challenges of graphene in biomedical applications. *Adv Mater*. 2013;25(16):2258–2268. doi:10.1002/adma.201203700
8. Verma S, Khanna V, Kumar S, Kumar S. The art of building living tissues: exploring the frontiers of biofabrication with 3D bioprinting. *ACS Omega*. 2023;8(50):47322–47339. doi:10.1021/acsomega.3c02600
9. Zare I, Mirshafiei M, Kheilnezhad B, et al. Hydrogel-integrated graphene superstructures for tissue engineering: from periodontal to neural regeneration. *Carbon N Y*. 2024;223:118970. doi:10.1016/j.carbon.2024.118970
10. Ghosal K, Mondal P, Bera S, Ghosh S. Graphene family nanomaterials- opportunities and challenges in tissue engineering applications. *FlatChem*. 2021;30:100315. doi:10.1016/j.flatc.2021.100315
11. Luo Z, Tang G, Ravanbakhsh H, et al. Vertical extrusion cryo(bio)printing for anisotropic tissue manufacturing. *Adv Mater*. 2022;34:12. doi:10.1002/adma.202108931
12. Ravanbakhsh H, Luo Z, Zhang X, et al. Freeform cell-laden cryobioprinting for shelf-ready tissue fabrication and storage. *Matter*. 2022;5(2):573–593. doi:10.1016/j.matt.2021.11.020
13. Magalhães LSSM, Santos FEP, Elias CDMV, et al. Printing 3D hydrogel structures employing low-cost stereolithography technology. *J Funct Biomater*. 2020;11(1):12. doi:10.3390/jfb11010012
14. Capella V, Rivero RE, Liaudat AC, et al. Cytotoxicity and bioadhesive properties of poly-N-isopropylacrylamide hydrogel. *Heliyon*. 2019;5(4):e01474. doi:10.1016/j.heliyon.2019.e01474
15. Mousseau Y, Mollard S, Qiu H, et al. In vitro 3D angiogenesis assay in egg white matrix: comparison to matrigel, compatibility to various species, and suitability for drug testing. *Lab Invest*. 2014;94(3):340–349. doi:10.1038/labinvest.2013.150
16. Mangir N, Dikici S, Claeysens F, MacNeil S. Using *ex ovo* chick chorioallantoic membrane (CAM) assay to evaluate the biocompatibility and angiogenic response to biomaterials. *ACS Biomater Sci Eng*. 2019;5(7):3190–3200. doi:10.1021/acsbomaterials.9b00172
17. Davern JW, Hipwood L, Bray LJ, Meinert C, Klein TJ. Addition of laponite to gelatin methacryloyl bioinks improves the rheological properties and printability to create mechanically tailorable cell culture matrices. *APL Bioeng*. 2024;8:1. doi:10.1063/5.0166206
18. Solecka U, Bajda T, Topolska J, Zelek-Pogudz S, Manecki M. Raman and Fourier transform infrared spectroscopic study of pyromorphite-vanadinite solid solutions. *Spectrochim Acta A Mol Biomol Spectrosc*. 2018;190:96–103. doi:10.1016/j.saa.2017.08.061
19. Esan DA, Trenary M. Interaction of CO with Pt nanoclusters on a graphene-covered Ru(0001) surface. *J Chem Phys*. 2021;154:11. doi:10.1063/5.0042686
20. Kaviani S, Talebi A, Labbaf S, Karimzadeh F. Conductive GelMA/alginate/polypyrrole/graphene hydrogel as a potential scaffold for cardiac tissue engineering: physiochemical, mechanical, and biological evaluations. *Int J Biol Macromol*. 2024;259:129276. doi:10.1016/j.ijbiomac.2024.129276
21. Li Y, Liu Y, Peng B, et al. Conductive, breathable and moisture-sensitive e-skin based on CNTs/graphene/GelMA mat for wound monitoring. *Biomater Adv*. 2022;143:213172. doi:10.1016/j.bioadv.2022.213172
22. Razmjooee K, Rashidy Ahmady A, Arabzadeh N, Ahmadi S, Saber-Samandari S, Toghraie D. Synthesis of gelatin/polyacrylamide/carboxymethyl chitosan triple-network hydrogels and evaluation of their properties for potential biomedical applications. *Mat Sci Eng*. 2023;295:116597. doi:10.1016/j.mseb.2023.116597
23. Mamidi N, Velasco Delgadillo RM, Barrera EV. Covalently functionalized carbon nano-onions integrated gelatin methacryloyl nanocomposite hydrogel containing  $\gamma$ -cyclodextrin as drug carrier for high-performance PH-triggered drug release. *Pharmaceuticals*. 2021;14(4):291. doi:10.3390/ph14040291
24. Özbaş Z, Torkay G, Bal-öztürk A, Özkahraman B. Preparation of quercetin incorporated photocrosslinkable methacrylated gelatin/methacrylated kappa-carrageenan antioxidant hydrogel wound dressings. *Chem Papers*. 2022;76(12):7597–7606. doi:10.1007/s11696-022-02426-3
25. Bayattork M, Rajkhowa R, Allardyce BJ, Wang X, Li J. Tuning the microstructure and mechanical properties of lyophilized silk scaffolds by pre-freezing treatment of silk hydrogel and silk solution. *J Colloid Interface Sci*. 2023;631:46–55. doi:10.1016/j.jcis.2022.11.003
26. Elliott WH, Bonari W, Maniglio D, Motta A, Tan W, Migliaresi C. Silk hydrogels of tunable structure and viscoelastic properties using different chronological orders of genipin and physical cross-linking. *ACS Appl Mater Interfaces*. 2015;7(22):12099–12108. doi:10.1021/acsami.5b02308

27. Chansoria P, Asif S, Polkoff K, Chung J, Piedrahita JA, Shirwaiker RA. Characterizing the effects of synergistic thermal and photo-cross-linking during biofabrication on the structural and functional properties of gelatin methacryloyl (GelMA) hydrogels. *ACS Biomater Sci Eng.* 2021;7(11):5175–5188. doi:10.1021/acsbomaterials.1c00635
28. Zhu Y, Yu X, Liu H, et al. Strategies of functionalized GelMA-based bioinks for bone regeneration: recent advances and future perspectives. *Bioact Mater.* 2024;38:346–373. doi:10.1016/j.bioactmat.2024.04.032
29. Das S, Jegadeesan JT, Basu B. Gelatin methacryloyl (GelMA)-based biomaterial inks: process science for 3D/4D printing and current status. *Biomacromolecules.* 2024;25(4):2156–2221. doi:10.1021/acs.biomac.3c01271
30. Zhang Y, Lv J, Zhao J, Ling G, Zhang P. A versatile GelMA composite hydrogel: designing principles, delivery forms and biomedical applications. *Eur Polym J.* 2023;197:112370. doi:10.1016/j.eurpolymj.2023.112370
31. Mamidi N, Ijadi F, Norahan MH. Leveraging the recent advancements in GelMA scaffolds for bone tissue engineering: an assessment of challenges and opportunities. *Biomacromolecules.* 2024;25(4):2075–2113. doi:10.1021/acs.biomac.3c00279
32. Rahali K, Ben Messaoud G, Kahn C, et al. Synthesis and characterization of nanofunctionalized gelatin methacrylate hydrogels. *Int J Mol Sci.* 2017;18(12):2675. doi:10.3390/ijms18122675
33. Siboro SAP, Anugrah DSB, Ramesh K, Park S-H, Kim H-R, Lim KT. Tunable porosity of covalently crosslinked alginate-based hydrogels and its significance in drug release behavior. *Carbohydr Polym.* 2021;260:117779. doi:10.1016/j.carbpol.2021.117779
34. Zhang X, Zhang H, Zhang Y, et al. 3D printed reduced graphene oxide-gelma hybrid hydrogel scaffolds for potential neuralized bone regeneration. *J Mater Chem B.* 2023;11(6):1288–1301. doi:10.1039/D2TB01979E
35. Nguta JM, Mbaria JM, Gakuya DW, Gathumbi PK. *Biological Scree I G of Ke Ya Medici Al Pla Ts Usi G Artemia Sali A L (ARTEMIIDAE)*. University of Nairobi; 2011:458–478.
36. Sanchez VC, Jachak A, Hurt RH, Kane AB. Biological Interactions of graphene-family nanomaterials: an interdisciplinary review. *Chem Res Toxicol.* 2012;25(1):15–34. doi:10.1021/tx200339h
37. Lee SH, Kang MS, Jeon S, et al. 3D Bioprinting of Human Mesenchymal Stem Cells-Laden Hydrogels Incorporating MXene for Spontaneous Osteodifferentiation. *Heliyon.* 2023;9.

International Journal of Nanomedicine

Dovepress

## Publish your work in this journal

The International Journal of Nanomedicine is an international, peer-reviewed journal focusing on the application of nanotechnology in diagnostics, therapeutics, and drug delivery systems throughout the biomedical field. This journal is indexed on PubMed Central, MedLine, CAS, SciSearch<sup>®</sup>, Current Contents<sup>®</sup>/Clinical Medicine, Journal Citation Reports/Science Edition, EMBase, Scopus and the Elsevier Bibliographic databases. The manuscript management system is completely online and includes a very quick and fair peer-review system, which is all easy to use. Visit <http://www.dovepress.com/testimonials.php> to read real quotes from published authors.

Submit your manuscript here: <https://www.dovepress.com/international-journal-of-nanomedicine-journal>